Quantifying the sensitivity of wind farm performance to array layout options using large-eddy simulation

Quantifying the sensitivity of wind farm performance to array layout options using large-eddy simulation

Cristina L. Archer,[1] Sina Mirzaeisefat,[1] and Sang Lee[2]

Received 27 June 2013; revised 21 August 2013; accepted 24 August 2013; published 23 September 2013.

[1] This paper attempts to quantify the effects of array layout on the performance of offshore wind farms. Array layout is characterized by the spacing between wind turbines (along and across the prevailing wind direction) and by their alignment (aligned or staggered). A large-eddy simulation code is utilized to create a turbulent boundary layer and is coupled with an actuator line model to simulate the effects of the rotating wind turbine blades. A control case (simulating the Lillgrund farm) and sensitivity runs are performed with various combinations of increased spacing, with and without staggering. Staggering every second row was found to be the simplest method to improve the capacity factor from 0.3 to 0.34 and array losses from 36% to 27%. The highest capacity factor (0.4) and the lowest array losses (14%) were obtained with a staggered layout with spacing across the prevailing wind direction that was twice the original. Smart layout choices can improve the array performance by 13%–33%. **Citation:** Archer, C. L., S. Mirzaeisefat, and S. Lee (2013), Quantifying the sensitivity of wind farm performance to array layout options using large-eddy simulation, *Geophys. Res. Lett.*, *40*, 4963–4970, doi:10.1002/grl.50911.

1. Introduction

[2] The layout of wind turbines can have an impact on the power production of a wind farm. Design variables that define the layout of wind turbines within a wind farm include: number of turbines; turbine model and diameter; orientation of the rows with respect to the prevailing wind direction (PWD); size and shape of the wind farm; spacing between turbines; and alignment of the turbines (i.e., whether in-line or staggered with one another).

[3] There are no universal layout recommendations for offshore wind farms, partly because isolating the contribution of each individual design variable is impossible at existing wind farms, where the wind turbines cannot be moved or removed to isolate the effect of individual design variables, and partly because analyzing the sensitivity to design variables requires sophisticated and computer-intensive numerical codes, such as large-eddy simulation (LES). In LES, the large-scale, unsteady, turbulent motions are resolved explicitly, whereas the effects of small-scale motions, as opposed to the motions themselves, are modeled via a subgrid model [*Pope*, 2000]. LES has been applied successfully to study turbine and array wake losses in recent years [e.g., *Calaf et al*., 2010; 2011; *Lu and Porté-Agel*, 2011; *Churchfield et al*., 2012b], as reviewed recently by *Archer et al*. [2013]. However, only a few LES studies have analyzed the effect of array layout explicitly, although none in a real wind farm. *Meyers and Meneveau* [2011] found that the optimal spacing in an idealized, infinite, nonstaggered wind farm was much higher than the spacing currently used in wind farms, although trade-offs were identified between the cost of the land and that of the wind turbine. *Wu and Porté-Agel* [2013] studied the effect of aligned and staggered wind farm layouts with 30 miniature turbines in a small wind tunnel and found that the staggered configuration lead to higher local wind speed and turbine efficiency. Similarly, *Stevens et al*. [2013] found an increase in power generation up to 40% by staggering wind turbines in an idealized wind farm.

[4] The National Renewable Energy Laboratory (NREL) developed the only publicly available and open-source LES code that is capable of resolving wind turbine blades as rotating actuator lines (not fixed disks) and does not rely on periodic boundary conditions. This code, named Simulator for Offshore/Onshore Wind Farm Applications (SOWFA; available at http://wind.nrel.gov/designcodes/simulators/sowfa/), has been used successfully in the past for turbulent wake simulations [*Churchfield et al*., 2010; 2012a; 2012b] and is the model of choice in this study.

[5] The SOWFA was used to simulate an existing offshore wind farm in Lillgrund (Sweden), consisting of 48 Siemens 2.3-megawatt (MW) turbines with the following specifications: rated power $P_R = 2300$ kilowatts (kW), a diameter (D) of 93 m, a 63.4-m hub height, spacing of 3.2D across and 4.3D along the PWD, and no staggering [*Dahlberg*, 2009]. This spacing is exceptionally tight; to our knowledge, it is the tightest of all modern wind farms. The prevailing wind direction at Lillgrund is from the southwest [*Bergstrom*, 2009], just as it is in the summer along most of the U.S. east coast, where several offshore wind farms are planned. Thus, the results of this study are highly applicable to the U.S. While keeping the area and the shape of the farm constant, three critical design variables were varied: number of turbines (N_T), turbine spacing (both along and across the PWD), and alignment (in-line or staggered for consecutive rows).

[6] The outcome of this study is a quantification of the advantages and disadvantages of various array layout choices. These estimates will be useful to the wind industry to optimize a wind project because the effects of alternative layouts can be quantified via array performance triangles with respect to total power, capacity factor, array losses, and number of wind turbines, all of which can ultimately be converted to actual costs or savings.

[1]College of Earth, Ocean, and Environment, University of Delaware, Newark, Delaware, USA.
[2]National Renewable Energy Laboratory, Golden, Colorado, USA.

Corresponding author: C. L. Archer, College of Earth, Ocean, and Environment, University of Delaware, Newark, DE 19716, USA. (carcher@udel.edu)

0094-8276/13/10.1002/grl.50911

2. Simulations

2.1. Model formulation

[7] Large-eddy simulation is performed to simulate the atmospheric boundary layer under constant surface roughness ($z_0 = 0.016$ m, typical of rough sea conditions) and neutral atmospheric stability. The incompressible formulations of the continuity, the momentum (which includes the Coriolis force, the buoyancy force, and the aerodynamic force at the actuator points), and the potential temperature equations are used as follows:

$$\frac{\partial \widetilde{u}_i}{\partial x_i} = 0 \tag{1}$$

$$\frac{\partial \widetilde{u}_i}{\partial t} + \frac{\partial(\widetilde{u}_i\widetilde{u}_j)}{\partial x_j} = -\frac{\partial \hat{p}}{\partial x_i} - \frac{\partial \tau_{ij}^D}{\partial x_j} - \frac{1}{\rho_0}\frac{\partial p_0(x,y)}{\partial x_i} - \varepsilon_{i3k} f_3 \widetilde{u}_k + g\left(\frac{\widetilde{\theta} - \theta_0}{\theta_0}\right)\delta_{i3} + \frac{1}{\rho_0}F_i \tag{2}$$

$$\frac{\partial \widetilde{\theta}}{\partial t} + \frac{\partial\left(\widetilde{u}_j\widetilde{\theta}\right)}{\partial x_j} = \frac{\partial q_j}{\partial x_j}\,. \tag{3}$$

The tilde on the velocity vector and potential temperature denotes the spatially resolved component. The modified pressure is defined as

$$\hat{p} = \frac{\widetilde{p}'}{\rho_0} + \frac{\tau_{kk}}{3} \tag{4}$$

where

$$\widetilde{p}'(x,y,z,t) = \widetilde{p}(x,y,z,t) - p_0(x,y) + \rho_0 g z\,. \tag{5}$$

The filtered static pressure is $\widetilde{p}$ and ρ_0 is the constant air density. The mean pressure term is $p_0(x,y)$, whose spatial gradient drives the flow. The last term $\rho_0 gz$ represents the hydrostatic pressure. The deviatoric part of the fluid stress tensor is

$$\tau_{ij}^D = \tau_{ij} - \frac{\tau_{kk}\delta_{ij}}{3} \tag{6}$$

where δ_{ij} is the Kronecker delta. The subgrid scale (SGS) stresses are included in the τ_{ij} term. The SGS flux is computed using the Smagorinsky model with a constant of 0.13 [*Smagorinsky*, 1963].

[8] The filter length scale is defined as $\Delta = (\Delta x \Delta y \Delta z)^{1/3}$, where Δx, Δy, and Δz are the local cell lengths along x, y, and z. The ε_{ijk} is the alternating unit tensor. The Coriolis parameter is defined as $f = 2\omega[0, cos(\varphi), sin(\varphi)]$, where ω is the planetary rotation rate (2.95×10^{-5} rad/s) and φ (55°N) is the latitude. The buoyancy effect is calculated using the Boussinesq approximation, where g is the gravity, θ is the resolved potential temperature, and θ_0 is the reference temperature taken to be 300 K. The last term, F_i, is the force generated by the actuator line model [*Sørensen and Shen*, 2002], discussed in the next paragraph. The transport equation for the resolved potential temperature equation is shown in equation (3), where q_j represents the temperature flux as

$$q_j = -\frac{\nu_{SGS}}{\mathrm{Pr}_{SGS}}\frac{\partial \widetilde{\theta}}{\partial x_j}, \tag{7}$$

where ν_{SGS} and Pr_{SGS} are the SGS viscosity and the turbulent Prandtl number following Moeng's formulation [*Moeng*, 1984; *Churchfield et al*., 2012a].

[9] The turbine model consists of an actuator line representation of the turbine blades [*Sørensen and Shen*, 2002]. Aerodynamic forces f_i^a at 40 equally spaced actuator points (x_j, y_j, z_j) are projected onto the flow field as the body force F_i in equation (2):

$$F_i = -\sum_{j=1}^{40} f_i^a\left(x_j, y_j, z_j, t\right)\frac{1}{\varepsilon^3\pi^{3/2}}\exp\left[-\left(\frac{\left|\vec{d}_j\right|}{\varepsilon}\right)^2\right], \tag{8}$$

where ε is the projection width and $\vec{d}_j$ is the distance from the actuator points such that the influence from the actuator points diminishes exponentially. The size of ε is equal to the chord length divided by 4.3 and varies along the radial direction of the blade. The actuator lines are modeled to mimic the Siemens 2.3-MW wind turbine, where the power calculations are based on the aerodynamic loads on the blades [*Churchfield et al*., 2012b].

[10] The above incompressible Navier-Stokes with the Coriolis force and the potential temperature flux equations (equations (1)–(3)) are solved using SOWFA, which is based on OpenFOAM libraries [*OpenFOAM*, 2011]. The equations are discretized using an unstructured collocated finite-volume formulation. A second-order central-differencing scheme is employed with the Rhie and Chow interpolation method [*Rhie and Chow*, 1983] to avoid checkerboard pressure-velocity decoupling. For the time advancement, Pressure Implicit Splitting Operation (PISO) is used, with three substep corrections to maintain a second-order temporal accuracy.

2.2. Domain Setup and Initialization

[11] The dimensions of the computational domain are 4 km by 4 km in the horizontal and 1 km in height, enough to cover the Lillgrund wind farm. The mesh resolution is ~7 m everywhere except in six blocks located around the wind turbines (shaded in Figure 1), where the resolution is ~3.5 m. The six blocks are necessary because of the "missing" turbines near the center of the farm (Figure 1a). This yielded a total of ~82 million grid cells. The simulations are initialized with a uniform wind speed of 9 m s^{-1} from the southwest and a temperature inversion based at 750 m. First, a precursor simulation is run for 14,000 s with periodic lateral conditions and no turbines to develop a fully turbulent boundary layer. The lateral values of wind speed and temperature are saved during the last 2000 s and used to provide lateral boundary conditions for the simulations with the wind turbines, which are started at 12,000 s. The time step varied between 0.07 and 0.3 s, depending on the Courant number. This initialization procedure, following *Churchfield et al*. [2012a], allows for the simulations with turbines to be effectively nonperiodic because the inlet boundary values are unaffected by the turbines themselves, as in the real world. The velocity spectra and the mean profiles from *Churchfield et al*. [2012a] correctly captured the inertial range and the law of the wall.

[12] All the LES simulations were run on the Mills high-performance computer cluster of the University of Delaware using 144 processors; on the average, each precursor run took a month of clock time, and each simulation with the

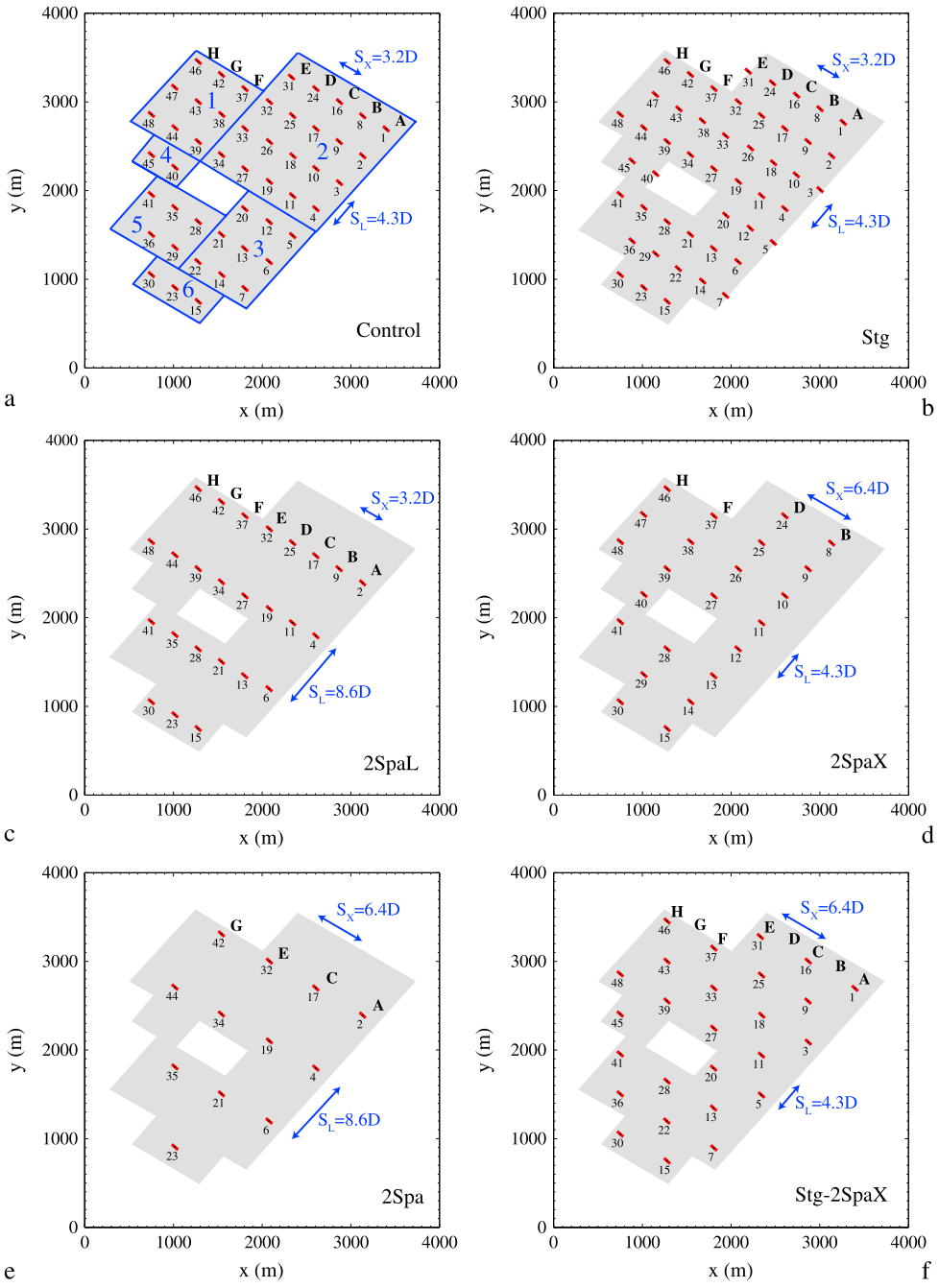

Figure 1. Array layouts used in the simulations: (a) original Lillgrund layout with 48 turbines and wind from the southwest, the prevailing direction (run name: Control); (b) same as Control but with turbines staggered every second row downwind (Stg); (c) same as Control but with double spacing along the prevailing wind direction (2SpaL); (d) same as Control but with double spacing across the prevailing wind direction (2SpaX); (e) same as Control but with double spacing both along and across the prevailing wind direction (2Spa); and (f) same as 2SpaX but staggered every second row downwind (Stg-2SpaX). The six subblocks with finer mesh refinement are shown as gray shaded areas (and with blue borders in Figure 1a).

turbines took two weeks, for a total of ~158,000 CPU-hours per case.

2.3. Simulation Details

[13] The Lillgrund offshore farm was chosen in this study because (1) it has already been successfully simulated with SOWFA [*Churchfield et al.*, 2010; 2012a; 2012b], (2) it was intentionally designed with a dense packing of wind turbines, thus making it ideal to study the effect of increased spacing, and (3) the PWD at Lillgrund, southwesterly, coincides with that along the U.S. east coast in the summer [*Hughes*, 2011; *Sheridan et al.*, 2012], thereby making this study relevant to the U.S. offshore industry. The original layout had a "hole" in the middle of the farm and not all the rows and columns had the same number of turbines (Figure 1a); both features were retained in this

Table 1. Settings and Performance Results of the Simulations for a Prevailing Wind Direction From the Southwest

Case name	Staggered	S_X	S_L	N_T	CF	AL (%)	P_{TOT} (MW)
Control	No	3.2D	4.3D	48	0.30	35.51	33.4
Stg	Yes	3.2D	4.3D	48	0.34	26.85	37.9
2SpaL	No	3.2D	8.6D	25	0.39	17.78	22.2
2SpaX	No	6.4D	4.3D	23	0.30	35.82	15.9
2Spa	No	6.4D	8.6D	12	0.38	17.89	10.6
Stg-2SpaX	Yes	6.4D	4.3D	26	0.40	14.45	24.0

S_L = spacing along the prevailing wind direction.
S_X = spacing across the prevailing wind direction.
N_T = number of turbines.
P_{TOT} = average power output from entire wind farm (MW).
CF = average capacity factor, calculated as P_{TOT} divided by $N_T \times 2.3$ MW.
AL = array losses.

study for consistency. The various runs are summarized in Table 1, and the layouts are visualized in Figure 1. The capacity factor of a single wind turbine is the ratio of its actual power over its rated power; for a wind farm, such as Lillgrund, it is the ratio of the total wind power from all the turbines P_{TOT} over the maximum power of the farm as follows:

$$CF = \frac{P_{TOT}}{N_T P_R} = \frac{\sum_{i=1}^{N_T} P_i}{N_T P_R}, \tag{9}$$

where P_i is the average power of each turbine over the simulation (2000 s).

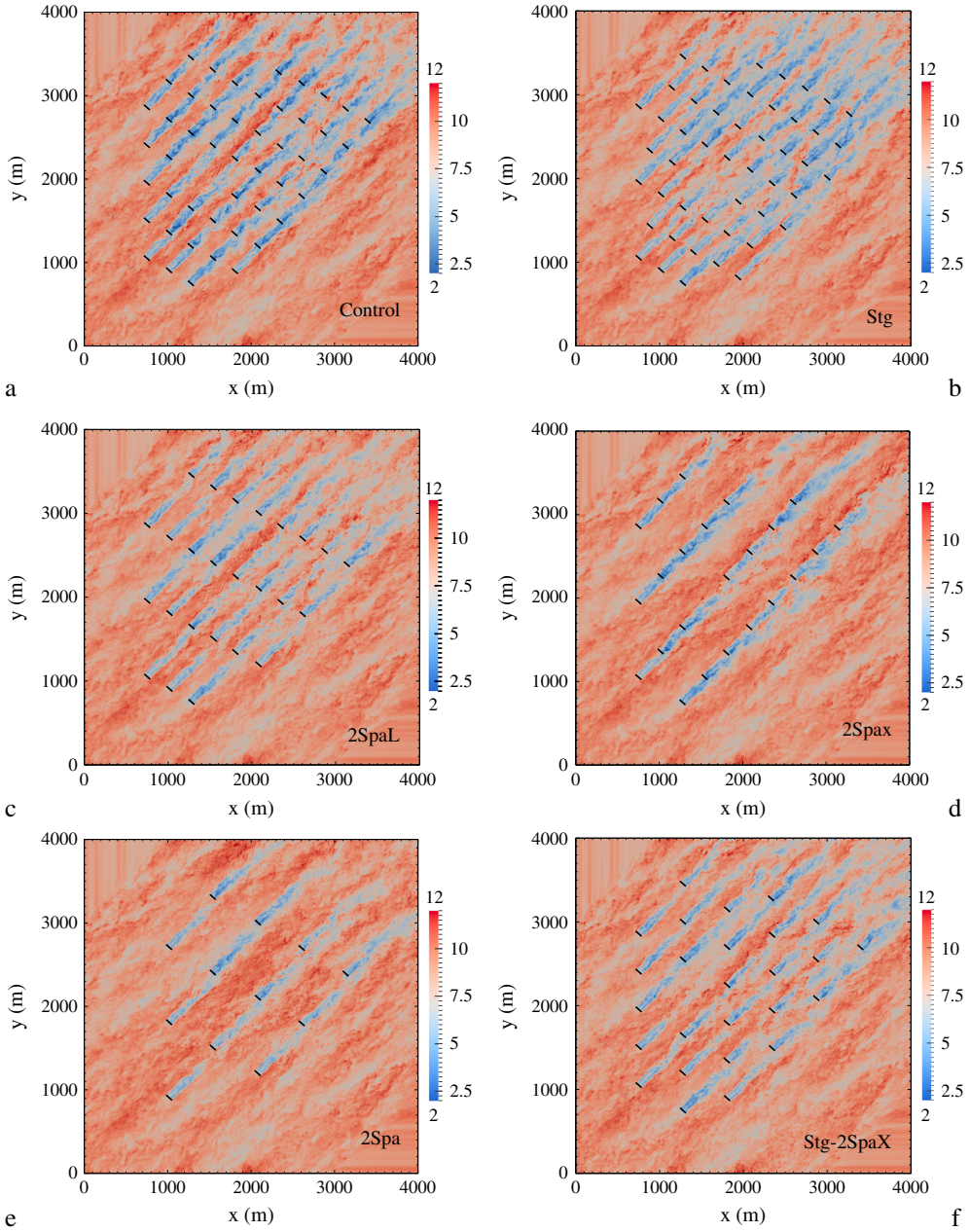

Figure 2. Horizontal cross sections of instantaneous wind speed (m s^{-1}) at 90 m above the ground at time t = 14,000 s for the same sensitivity runs as in Figure 1.

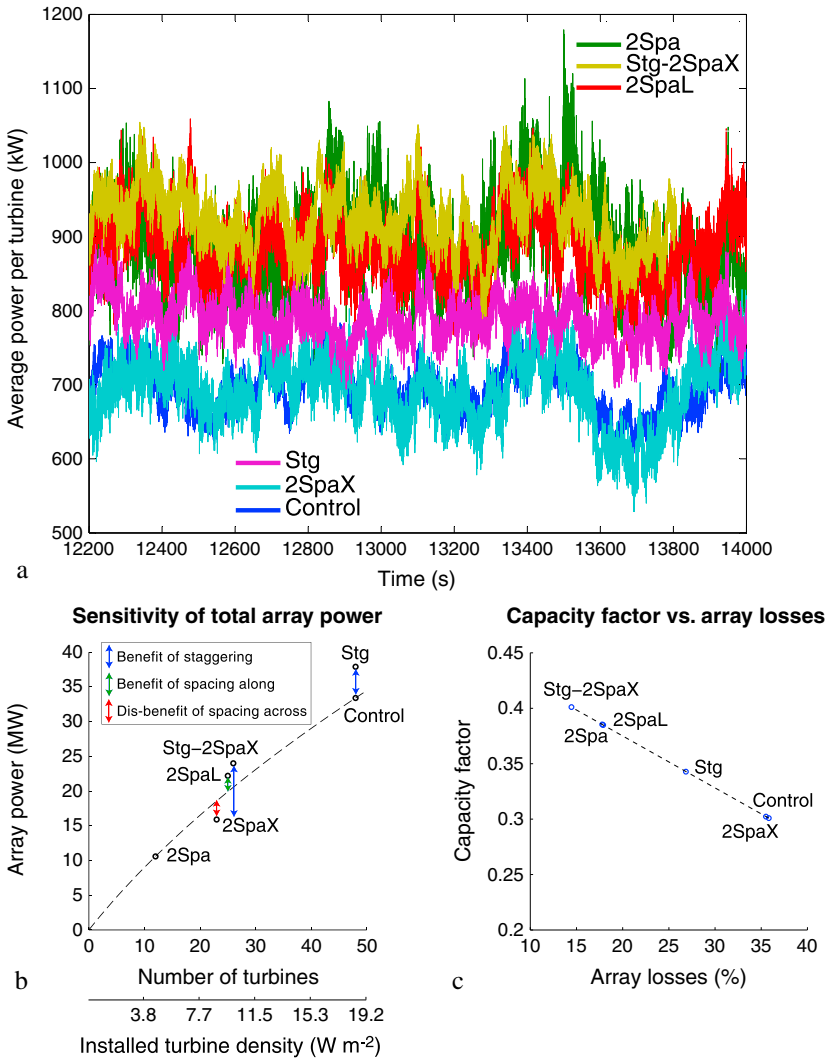

Figure 3. Array performance assessment: (a) time series of average power per turbine (kW), (b) total array power (MW) as a function of number of turbines (or installed turbine density in W m^{-2}), and (c) relationship between capacity factor and array losses. The dashed line in Figure 3b is an empirical fit that represents arrays in which the spacing across and along are changed by the same factor simultaneously (e.g., both spacings are doubled from Control to 2Spa). The benefits of staggered configurations in Figure 3b (runs Stg and Stg-2SpaX) are obtained from the nearest nonstaggered configuration (Control and 2SpaX, respectively). The dashed line in Figure 3c shows the linear fit between array losses (AL) and capacity factor (CF). The fitting equation is $CF = -0.0047 \times AL + 0.47$, where AL is in percent.

[14] Because the farm area was kept constant (6 km^2 including the "hole"), any change in the spacing along (S_L) or across (S_X) the PWD caused a change in the number of installed turbines (N_T). When possible, the turbines were kept in the same row (1–7 and 15) and column (A–H) as in run Control. A staggered layout is defined here by its closest nonstaggered configuration with a shift in every other row by half S_X. For example, the layouts in Stg and Stg-2SpaX are obtained from those in Control and 2SpaX but with the even rows shifted by $0.5 \times 3.2D$ and $0.5 \times 6.4D$, respectively. Because of the nonuniform original layout, N_T in Stg-2SpaX is slightly higher than in 2SpaX (26 versus 23).

3. Results

3.1. Wakes

[15] A wind turbine wake is the region downwind of a turbine in which the wind speed is lower and turbulent kinetic energy (TKE) is higher than upwind. In wind farms, multiple wakes can overlap and their interactions are not linear. Examples of the simulated wakes for the various layout options at Lillgrund are in Figure 2, in which the horizontal cross sections of instantaneous wind speed are taken at 90 m above ground at t = 14,000 s. The boundary layer has evolved from its initial uniform state into a turbulent state with average wind speeds between 7.5 and 12 m s^{-1} outside of the wind farm region. Inside the farm, the wakes are shown as blue streaks of wind speeds lower than the surrounding values, as low as 2 m s^{-1} at a few points. The highest deficits in wind speed are found in the Control, Stg, and 2SpaX runs.

[16] The wakes did not spread much laterally but lingered downwind for distances greater than the spacing along. Although the domain did not extend far enough to simulate the wakes from the last turbine rows, it appears that within $2S_L = 8.6D$, the wakes have mostly dissipated (Figures 2c and 2e).

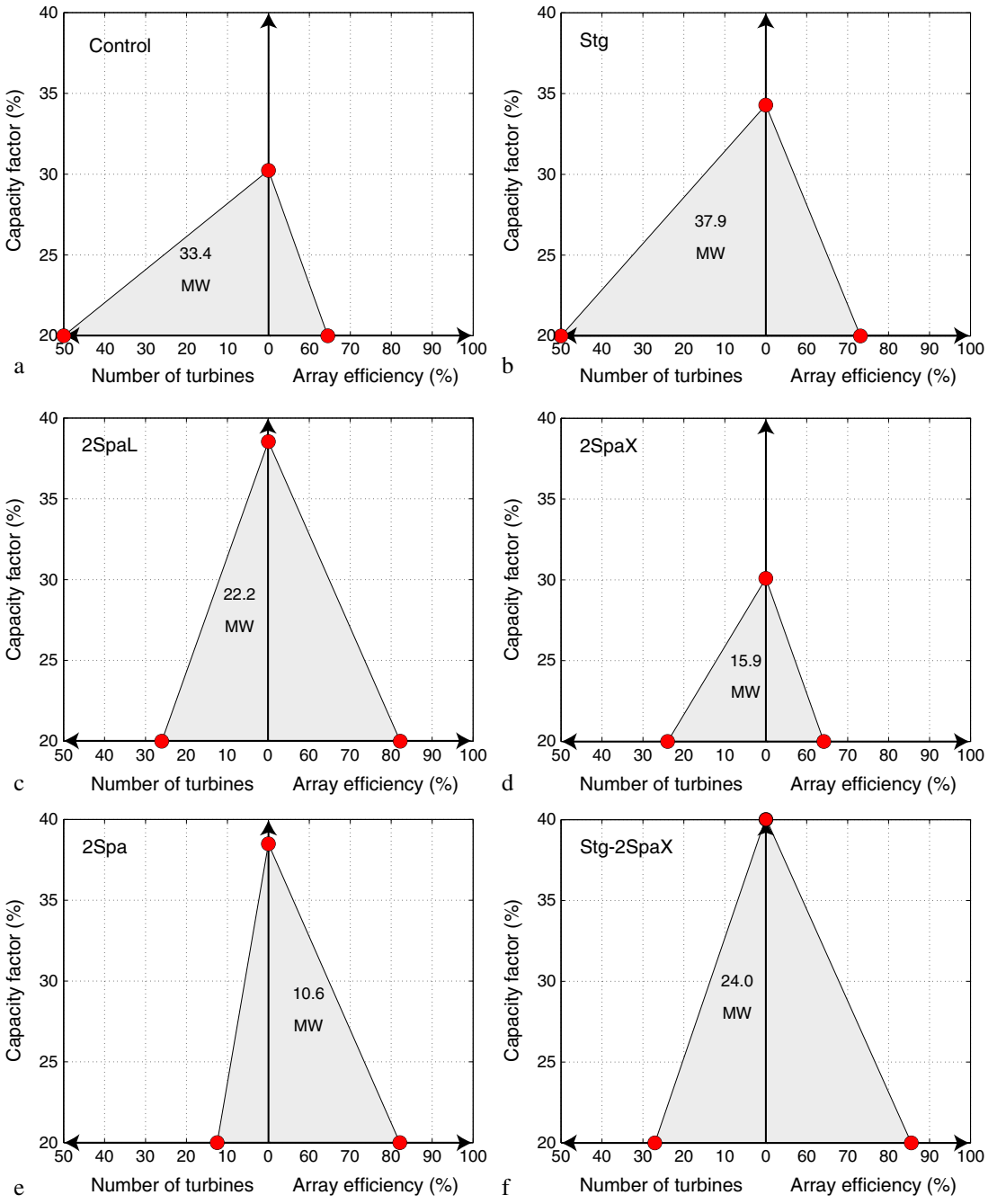

Figure 4. Array performance triangles for the simulations, displaying number of turbines, array efficiency, and capacity factor (CF) for each case, using the Siemens 2.3-MW wind turbine. The total array power in megawatts (MW) is also displayed.

[17] In several cases, the highest wind speeds were found inside, not outside, of the wind farm, which suggests that constructive interferences can occur between wakes. This nonlinear effect is found near turbines 25–27 in the Control, 2SpaL, 2SpaX, and 2Spa runs (Figures 2a, 2c, 2d, and 2e).

3.2. Wind Power Output and Array Losses

[18] The average wind power output per wind turbine (P) for all cases is shown in Figure 3a. Because of the dense packing in the Control run, the average power per turbine was low (695 kW), yet easily improved with all layout choices except for 2SpaX. This suggests that the original lateral spacing between adjacent turbines S_X was sufficient to contain the turbine wakes such that increasing it yielded negligible benefits. The highest average powers were obtained with the 2Spa and 2SpaL runs, which outline the beneficial effect of increasing the spacing along the PWD, consistent with *Meyers and Meneveau* [2011]. With the same number of turbines as the Control, the run Stg produced an impressive 789 kW of average power, with an improvement in the capacity factor (CF) from 0.3 to 0.34 (Table 1), which supports similar findings by *Wu and Porté-Agel* [2013] and *Stevens et al.* [2013].

[19] Because the number of turbines varies as turbine spacing and staggering are changed, the total power output of the

array depends on the array layout as well (Figure 3b). Because of nonlinear effects, the total array power does not increase linearly with the number of turbines. For example, doubling the spacing along and across the PWD in run 2Spa implies that only one quarter of the turbines (12) are used with respect to the Control case (48), but the power output (10.6 MW) is higher than one quarter of the Control's (33.4 MW), thus the higher CF (Table 1). The benefits of staggering are obtained by comparing the results from staggered layouts (runs Stg and Stg-2SpaX) to those from the closest nonstaggered ones (Control and 2SpaX), even though N_T may not be exactly the same.

[20] An empirical fit representing the performance of arrays in which both S_L and S_X are varied by the same factor is shown with a dashed line in Figure 3b. The line was obtained by imposing that the first derivative be equal to the capacity factor for runs 2Spa and Control, for which the spacing along and across were varied by a factor of two. For a given number of turbines N_T, this line allows for the comparison of the benefits of the layout choices that are not equal in both directions along and across the PWD, such as runs 2SpaX and 2SpaL. Figure 3b shows that, whereas increasing S_L is beneficial (green arrow), increasing S_X is not (red arrow), unless the increase in S_X is accompanied by staggering (blue arrow).

[21] Array losses are defined here as follows. The average power generated by the three turbines (15, 23, and 30; Figure 1a) in the front row of the Control run is $P_0 = 1{,}078$ kW and represents the power that would be generated at Lillgrund in the absence of wake losses. This power corresponds to a capacity factor $CF_0 = 1078/2300 = 0.47$. For each layout, the average power per turbine (P) is calculated (Figure 3a), and the array efficiency η is given by the ratio P/P_0. Array losses (AL) are defined as

$$AL = 1 - \frac{P}{P_0} = 1 - \eta \,. \tag{10}$$

Because $P = CF \times P_R$, where P_R is the rated power (2300 kW), the relationship between AL and the CF is linear (Figure 3c) and does not depend on the array layout. For the Control case, in which the turbines were extraordinarily packed, the final CF was 0.3, substantially lower than $CF_0 = 0.47$, due to the 36% array losses. For runs 2SpaL and Stg-2SpaX, which had turbine spacings of $6.4D \times 4.3D \sim 27D^2$, similar to those found in average wind farms ($7D \times 4D = 28D^2$), the CF was 0.39–0.4 with AL = 14%–18%.

3.3. The Array Performance Triangles

[22] Array performance triangles (APTs) are introduced here (Figure 4) to visualize the four variables that describe the wind farm performance: CF, N_T, AL (or η), and the total power output P_{TOT}. The information in Figure 4 is the same as that in Table 1, but it is more immediate and visually appealing. The slope of the right side of the APTs is constant for all the runs because of the linear relationship between CF and AL described earlier. This slope can vary for different wind turbines, wind regimes, and atmospheric stability. The slope of the left side of the APTs generally gets steeper as N_T decreases because the CF generally improves with a lower number of wind turbines. The total area of the APT is roughly proportional to the overall performance of the array, which is proportional (although not linearly) to all three variables N_T, η, and CF. Whereas an exact definition of the overall array performance depends on the weights assigned to each of the three variables, which depend on complex economic, political, and environmental considerations that are beyond the scope of this research, the APTs allow for a qualitative evaluation of it because larger areas reflect simultaneous improvements in all three variables and therefore an overall improved array performance. The area of the left square-triangle in each APT is exactly proportional to one-half P_{TOT} (value shown in MW). If maximizing total array power output is the goal, then the layout of Stg is the appropriate choice because it has the largest left square-triangle of all APTs. If overall array performance is the goal, then Stg-2SpaX stands out because it has the biggest APT.

4. Conclusions and Future Work

[23] Large-eddy simulations coupled with an actuator line model were performed to investigate the impact of wind farm layout on wind power production. Six different configurations of a wind farm in Lillgrund, Sweden, were studied by varying the spacing between adjacent turbines (along and across the prevailing wind direction) and staggering their positions. Staggering every second row increased the wind farm's capacity factor from 0.3 to 0.34 and maximized total power production by allowing every second row of turbines to receive higher wind velocity than in the Control case. Increasing the turbine spacing in the predominant wind direction to enhance wake recovery and combining that with staggering every second row yielded the highest capacity factor (0.4) with lowest array losses (14%).

[24] The present work is limited to neutral atmospheric stability and to the prevailing wind direction, partly due to the high computational costs associated with these simulations (>100,000 CPU-hours per run). The sensitivity of these findings to different atmospheric stabilities and wind directions will be studied in a subsequent paper.

[25] **Acknowledgments.** Part of this research was funded by the University of Delaware Research Foundation.

[26] The Editor thanks two anonymous reviewers for assistance evaluating this manuscript.

References

Archer, C. L., et al. (2013), Meteorology for coastal/offshore wind energy in the United States: recommendations and research needs for the next 10 years, *Bull. Am. Meteorol. Soc.*, doi:10.1175/BAMS-D-13-00108.1.

Bergstrom, H. (2009), Meteorological conditions at Lillgrund, *Swedish Energy Agency*, 1–26.

Calaf, M., C. Meneveau, and J. Meyers (2010), Large eddy simulation study of fully developed wind-turbine array boundary layers, *Phys. Fluids*, *22*(1), 015110, doi:10.1063/1.3291077.

Calaf, M., M. B. Parlange, and C. Meneveau (2011), Large eddy simulation study of scalar transport in fully developed wind-turbine array boundary layers, *Phys. Fluids*, *23*(12), 126603, doi:10.1063/1.3663376.

Churchfield, M. J., G. Vijayakumar, J. G. Brasseur, and P. J. Moriarty (2010), *Wind Energy-Related Atmospheric Boundary Layer Large-Eddy Simulation Using OpenFOAM*, Keystone, Colo.

Churchfield, M. J., S. Lee, J. Michalakes, and P. J. Moriarty (2012a), A numerical study of the effects of atmospheric and wake turbulence on wind turbine dynamics, *J. Turbul.*, *13*(14), 1–32.

Churchfield, M. J., S. Lee, P. J. Moriarty, L. A. Martinez, S. Leonardi, G. Vijayakumar, and J. G. Brasseur (2012b), *Large-Eddy Simulations of Wind-Plant Aerodynamics*, pp. 1–19, Nashville, Tenn.

Dahlberg, J. A. (2009), Assessment of the Lillgrund windfarm, Swedish Energy Agency.

Hughes, C. (2011), The climatology of the Delaware Bay/sea breeze, 1–129 pp., University of Delaware, Newark (DE). [online] Available from: http://udspace.udel.edu/bitstream/handle/19716/10659/Christopher_Hughes_thesis.pdf

Lu, H., and F. Porté-Agel (2011), Large-eddy simulation of a very large wind farm in a stable atmospheric boundary layer, *Phys. Fluids*, *23*(6), 065101, doi:10.1063/1.3589857.

Meneveau, C. (2012), Large eddy simulations of large wind-turbine arrays in the atmospheric boundary layer, *J. Turbul.*, *13*(7), 1–12, doi:10.1080/14685248.2011.663092.

Meyers, J., and C. Meneveau (2011), Optimal turbine spacing in fully developed wind farm boundary layers, *Wind Energy*, *15*(2), 305–317, doi:10.1002/we.469.

Moeng, C. H. (1984), A large-eddy-simulation model for the study of planetary boundary-layer turbulence, *J. Atmos. Sci.*, *41*, 2052–2062.

OpenFOAM (2011), The open source CFD toolbox, User Guide, 2nd ed., OpenFOAM Foundation. [online] Available from: http://www.openfoam.org/docs/user

Pope, S. B. (2000), *Turbulent Flows*, Cambridge Univ. Press, Cambridge, UK.

Rhie, C. M., and W. L. Chow (1983), Numerical study of the turbulent flow past an airfoil with trailing edge separation, *AIAA J.*, *21*, 1525–1532.

Sheridan, B., S. D. Baker, N. S. Pearre, J. Firestone, and W. Kempton (2012), Calculating the offshore wind power resource: Robust assessment methods applied to the U.S. Atlantic coast, *Renewable Energy*, *43*, 224–233, doi:10.1016/j.renene.2011.11.029.

Smagorinsky, J. (1963), General circulation experiments with the primitive equations, *Mon. Weather Rev.*, *91*, 99–164.

Sørensen, J. N., and W. Z. Shen (2002), Numerical modeling of wind turbine wakes, *J. Fluids Eng.*, *124*(2), 393–399.

Stevens, R. J. A. M., D. F. Gayme, and C. Meneveau (2013), *Effect of turbine alignment on the average power output of wind farms*, pp. 1–12, Lyngby, Denmark.

Wu, Y.-T., and F. Porté-Agel (2013), Simulation of turbulent flow inside and above wind farms: Model validation and layout effects, *Boundary-Layer Meteorol.*, *146*(2), 181–205, doi:10.1007/s10546-012-9757-y.